Dynamics of Water Dissociative Chemisorption on Ni(111): Effects of Impact Sites and Incident Angles

Bin Jiang and Hua Guo

Phys. Rev. Lett. **114**, 166101 — Published 20 April 2015

DOI: 10.1103/PhysRevLett.114.166101

Submitted to PRL, 1/7/2015

Dynamics of Water Dissociative Chemisorption on Ni(111): Effects of Impact Sites and Incident Angles

Bin Jiang[a] and Hua Guo[a,b,*]

[a]Department of Chemistry and Chemical Biology, University of New Mexico, Albuquerque, New Mexico 87131

[b]Department of Physics and Astronomy, University of New Mexico, Albuquerque, New Mexico 87131

PACS numbers: 31.50.-x, 34.50.Lf, 68.43.-h, 68.49.-Bc, 82.65.+r

*: corresponding author: hguo@unm.edu

Abstract

The dissociative chemisorption of water on rigid Ni(111) is investigated using a quasi-classical trajectory method on a nine-dimensional global potential energy surface based on a faithful permutation invariant fit of ~25,000 density functional theory points. This full-dimensional model not only confirms the validity of our earlier reduced-dimensional model with six degrees of freedom, but also allows the examination of the influence of impact sites and incident angles. It is shown that the reactivity depends on the site of impact in a complex fashion controlled by the topography of the potential energy surface, rather than the barrier height alone. In addition, the reaction is promoted by momenta both parallel and perpendicular to the surface, as predicted by the recently proposed Sudden Vector Projection model.

In the past decades, tremendous progress has been made in understanding the interaction of molecules with solid surfaces.[1] This is particularly true for dissociative chemisorption,[2, 3] a key and often rate-limiting step in heterogeneous catalysis. Indeed, the dissociative chemisorption of H_2 is now mostly understood,[4, 5] and as a result recent attention has shifted to polyatomic molecules, such as methane and water.[3, 6, 7] For such processes, quantum state-resolved molecular beam experiments have been instrumental in revealing non-statistical dynamics such as mode specificity and bond selectivity.[8-16] However, theoretical understanding of these state-of-the-art experiments is still lagging.[3, 7] One of the major stumbling blocks is the lack of accurate high-dimensional global potential energy surfaces (PESs) for the molecule-surface interaction. Despite many efforts,[16-21] most of the existing PESs either ignore the surface periodicity and/or the permutation symmetry of identical atoms in the molecule, or lack high accuracy and global smoothness. Although the *ab initio* molecule dynamics (AIMD) approach, which requires no PES, has been employed to study the dynamics,[22, 23] it is still too expensive to compute sticking coefficients as low as 10^{-6} measured in many experiments. Consequently, accurate and efficient global PESs with correct symmetry properties suitable for quasi-classical trajectory (QCT) and/or quantum dynamical (QD) calculations are highly desired for polyatomic dissociative chemisorption processes.

In this Letter, we focus on the dissociative chemisorption of water on Ni(111), which is an essential step in many industrial processes such as steam reforming and the water-gas shift reaction.[24, 25] Very recently, the first quantum-state resolved

experiment on the dissociative chemisorption of D_2O on Ni(111) has been reported,[16] revealing a strong enhancement of reactivity by exciting the anti-symmetric stretch (v_3) of D_2O. The mode specificity was semi-quantitatively understood using our six-dimensional (6D) quantum model,[16, 19, 26] which neglects two lateral surface coordinates and the azimuthal angle. However, many uncertainties remain. For example, the validity of this reduced-dimensional model in describing the mode specificity has not been established. Nor is it clear how the impact site and angles of the incident molecule affect the dissociation. To achieve a better understanding, we report here the first globally accurate PES in full nine dimensions (9D) for water dissociative chemisorption on the rigid Ni(111) surface. Since a fully coupled 9D quantum treatment of this system is still formidable, we report here a QCT study of D_2O dissociative chemisorption on this PES to shed light on the site and angle dependences of the dynamics for this important reaction.

To develop the 9D PES, spin-polarized plane-wave density functional theory (DFT) calculations were performed using the Vienna Ab initio Simulation Package (VASP).[27, 28] The Ni(111) surface is represented by a slab model with a 3×3 unit cell and four Ni layers. The top two layers are optimized without the adsorbate and kept in their equilibrium positions. The interaction between the ionic cores and electrons was represented by the projector-augmented wave (PAW) method[29] with a kinetic energy cutoff at 350 eV. The Brillouin zone was sampled using Monkhorst-Pack scheme and a 3×3×1 *k*-points grid mesh.[30] The generalized gradient approximation (GGA) was used to treat the electron exchange-correlation

effects,[31] with the Perdew-Wang (PW91) functional.[32] More details about the DFT calculations and additional results can be found in our recent work[16, 33] and in Supporting Material (SM).

To provide an analytical representation of the DFT points, the recently proposed permutationally invariant polynomial-neural network (PIP-NN) fitting approach was used, which guarantees the surface and permutation symmetries intrinsic in the system.[34] In the PIP-NN approach for gas phase species, the symmetry functions in the form of low-order PIPs[35] serve as the input layer of the NN.[36, 37] A similar strategy can be used for molecule-surface interaction PESs when the PIPs are defined in terms of functions with surface periodicity.[34] The efficiency and accuracy of the PIP-NN approach has been recently demonstrated for the H_2/Ag(111) system.[38]

To reduce the complexity of the PES, an approximate C_{6v} symmetry is assumed for the fcc and hcp hollow sites, which thus become indistinguishable in the PES. This is a reasonable approximation for the (111) metal surface due to the small energy differences between the two sites.[39] With this approximation, the primitive symmetry functions are defined as follows:

$$G_{3i+1} = \left[\cos(\frac{4\pi y_i}{a\sqrt{3}}) + 2\cos(\frac{2\pi x_i}{a})\cos(\frac{2\pi y_i}{a\sqrt{3}}) \right] \exp(-\lambda z_i), \quad (1)$$

$$G_{3i+2} = \left[\cos(\frac{4\pi x_i}{a}) + 2\cos(\frac{2\pi x_i}{a})\cos(\frac{2\sqrt{3}\pi y_i}{a}) \right] \exp(-\lambda z_i), \quad (2)$$

$$G_{3i+3} = \exp(-\lambda z_i), \quad (3)$$

where i=0, 1, 2, and 3 are for the center of mass (COM) of H_2O, H, H, and O atoms,

respectively. The *z*-dependent terms in Eqs. (1-2) are needed to guarantee the flatness of the asymptotic potential at large *z* values. In addition, the following terms of the internuclear distances for H_2O are also needed:

$$G_{13} = \exp(-\lambda r_{12}), \quad (4)$$

$$G_{14} = \exp(-\lambda r_{13}), \quad (5)$$

$$G_{15} = \exp(-\lambda r_{23}). \quad (6)$$

As discussed previously,[34] these 15 primitive symmetry functions intrinsically include the C_{6v} symmetry of the (111) surface, and the permutation symmetry of the two H atoms is further provided by PIPs of G_4 -G_{15}, resulting in 21 symmetric functions for the input layer of the NN, as detailed in SM. To sample the configuration space, we started from a set of initial geometries mainly selected along the reaction pathway with low energies, then fit these points to a primitive PES using the PIP-NN method with fewer neurons.[34] Classical trajectories were launched on this PES to generate more points, from which those satisfying both energy and geometry criteria (see SM) were added to the data set. The enlarged data set is then used to generate the next generation of the PES using the same fitting procedure with more neurons. This procedure was iterated until few new points can be added and the reaction probability becomes converged. More details of the PIP-NN fitting and sampling strategy can be found in our recent work[34, 38] and in SM.

A total of 25,383 points was collected. They were divided randomly into the data (90%), validation (5%) and test (5%) sets to avoid over-fitting, and fit with an NN with 40 and 60 neurons in the first and second hidden layers, yielding 3401

parameters in total. The final PES is an average of the best three fits, leading to the overall root mean square error (RMSE) of 0.02 eV. This unprecedented fitting accuracy, which is considerably better than those reported in previous polyatomic-surface PESs,[16, 18, 19, 40] reflects the prowess of the PIP-NN approach. More details in SM demonstrate the accuracy and convergence of the PES.

QCT calculations were performed on the 9D PES using a modified VENUS program[41] to study the dissociation dynamics.[38, 42] The initial COM of D_2O (z_0) was chosen at 10.0 Å above the surface, with its lateral coordinates (x_0 and y_0) randomly sampled in the unit cell. The initial incident angle, defined as the colatitude angle θ for the z axis (surface normal), was fixed while the azimuthal angles φ was randomly sampled. The initial momentum p of the COM was determined by the translational energy E_i: $p = \sqrt{2ME_i}$ with M as the total mass of D_2O, and pointing towards the surface along the incident angle. The vibrational mode specificity in normal incidence (θ=0°) was investigated by sampling the rotationless D_2O in the three normal modes.[43] The integration time step was selected to be 0.10 fs and all trajectories conserved energy within 0.1 meV. Up to 1×10^6 trajectories were calculated at each translational energy, resulting in statistical uncertainty of a few percents. A trajectory is deemed reactive if the longer O-H distance is larger than 2.2 Å. Since the surface lattice effects[7] were not included in the present calculations, a direct comparison with experimental sticking coefficients was not attempted. The mode specificity, nonetheless, is not expected to change much when the lattice effects are included, as found in previous studies.[16, 40]

With this 9D PES, it becomes possible to explore the dependence of reactivity on surface sites, which is infeasible on the previous 6D model.[16] Figure 1a shows barrier heights as the molecular COM is fixed at different sites in the (111) irreducible cell with the assumed C_{6v} symmetry. It is important to note that the transition state is not exactly on the top site but shifted somewhat towards the bridge site, which is in accord with DFT calculations. Although the barrier height does depend on the site, it cannot be simply approximated by a harmonic model, as pointed out recently by Jackson and coworkers.[23] In addition, contour plots of the PES as a function of the vertical coordinate of COM (z_0) and the distance between dissociating H atom and COM (r) with other coordinates fully relaxed are shown in Figures 1(b-d) for dissociation fixed at the top, bridge, and hcp sites, respectively. These contour plots not only confirm the global smoothness of the PES, but also highlight the differences of the potential topography at different sites. Although the top site has a lower barrier height, interestingly, it has a tight saddle point lying almost perpendicular to the approaching coordinate z_0, resulting in a very small reaction probability due to the ineffectiveness in converting the incident energy to overcome the barrier. On the other hand, the barriers at the bridge and hcp sites are higher but much looser, which might contribute to the overall reactivity at high energies despite the higher barrier. To validate this point, we analyzed the initial lateral positions of the reactive trajectories in normal incidence at different translational energies and the results are displayed in Figure 2. At E_t=14 kcal/mol, which is just above the vibrationally adiabatic barrier, the reactive trajectories are mostly located near the center of the triangle, i.e.

x_0=[0.3-1.0] Å, where the barrier height is the lowest as shown in Figure 1a. With the increase of translational energy, more and more reactive trajectories appear near the hcp site. The distribution at E_t=20 kcal/mol shifts further to the right side of the irreducible triangle, particularly favoring the hcp site, suggesting that the dissociation is dominated by the loose saddle point there. Interestingly, trajectories initiated near the top site are almost always non-reactive even though the top site barrier height is 0.13 eV lower than that on hcp site, which is very similar to the HCl/Au(111) system where the dissociation probability on the top site is 100 times smaller than that on other sites.[44] These observations suggest that the simple energy shifting site-average model[23, 45] used in many previous studies may not be quantitatively accurate. A more rigorous treatment is to average fixed-site reaction probabilities on multiple high symmetric sites, as done recently for H_2/Cu(111)[46] and HCl/Au(111).[44]

In Figure 3a, dissociation probabilities calculated on the 9D PES for the ground and several vibrational excited states of D_2O are displayed. It is clear that excitations in all three vibrational modes as well as in the translational mode promote the dissociative adsorption significantly, in agreement with our previous results with reduced-dimensional models.[16, 19] In addition, the vibrational excitations enhance the reaction more effectively than translational excitation, as shown in Figure 3b, where the probabilities are plotted as a function of total energy. Quantitatively, the vibrational efficacy defined as $\eta = \left[E_t(0,P_0) - E_t(v,P_0)\right]/\Delta E_v$, where ΔE_v is the vibrational excitation energy and $E_t(0,P_0) - E_t(v,P_0)$ is the translational energy

difference at a given dissociation probability for the ground and excited vibrational states,[9] is found to depend on translational energy. For example, η for the symmetric stretching (v_1), bending (v_2), and anti-symmetric stretching (v_3) modes range from 1.50~1.85, 1.19-1.46, and 1.40~1.60, respectively, all larger than unity. These results are in general accord with previously reported 6D QD results,[16] and those obtained in QCT calculations using the original PW91 6D PES, as also shown in Figures 3a-3b, but the 6D QCT results appear to underestimate the v_1 efficacy while overestimate that for the v_2 mode. We note that QD probabilities are generally consistent with QCT contourparts using the same 6D PES (See Fig. S6 in SM). The results in Figure 3 confirm that the 6D model represents a semi-quantitative approximation of the dissociative chemisorption.

The mode specificity observed in both 9D and 6D calculations can be readily understood by the recently proposed Sudden Vector Projection (SVP) model,[40, 47-49] which assumes that the reaction occurs instantaneously prior to any intramolecular vibrational energy redistribution (IVR) in the impinging molecule. This is a reasonable approximation for water or methane,[23, 50] which has a sparse density of states. In this sudden limit, the enhancement of reactivity of a reactant mode is related to its coupling with the reaction coordinate at the transition state, which is estimated in the SVP model by the projection of the reactant mode vector ($\vec{Q}_i$) onto the reaction coordinate vector at the transition state ($\vec{Q}_{RC}$), denoted as $P_i = \vec{Q}_i \cdot \vec{Q}_{RC} \in [0,1]$. As discussed in our recent SVP studies,[33] both stretching modes of water have identical SVP values (P_i=0.67), which are larger than that (P_i

=0.24) for translation along the surface normal, consistent with the results reported here. The effect of bending mode seems to be underestimated in SVP model, due presumably to its much smaller frequencies allowing faster IVR.[49]

Interestingly, the SVP model also predicted a dependence of reactivity on the incident angles.[33] The translational vectors parallel to the surface were found to have non-negligible overlaps with the reaction coordinate vector (P_i=0.03/0.14), comparing to P_i=0.24 of that along the surface normal. To investigate the effect of the incident angles on the reaction probability, we carried out two types of simulations at three experiment nozzle temperatures.[16] In our simulations, the vibrational and rotational modes of D_2O are thermalized at the nozzle temperature and 22 K, respectively. In the first set of simulations, the total translational energy E_t is fixed to the experimental value, and the incident angle θ is scanned from 0° (surface normal) to 60^o. It is shown in Figure 4a that the reaction probability decreases with the increase of the incident angle (and the decrease of normal incident energy). This indicates that the translational energy along the surface normal promotes the reaction, consistent with the SVP prediction of its large projection onto the reaction coordinate. In the second set of calculations, the normal component of the incident energy $E_n=E_t\cos^2(\theta)$ is fixed as the angle varied. As shown in Figure 4b, the reaction probability is found to increase gradually with the increasing incident angle from $\theta=0^o$ to 45^o, but level off at 60^o. Interestingly, the enhancement of the translational energy along the surface plane is higher at lower nozzle temperatures. For example, the dissociation probability at 573 K is about nine times greater at $\theta=60^\circ$ than that at normal incidence. These results

underscore a small but significant influence of the translation energy parallel to the surface. The situation here is similar to the deviation from the normal scaling in methane dissociative sticking on Ni(100),[51] which was also predicted by the SVP model.[23]

To summarize, we report here a 9D global PES based on a PIP-NN fit of a large number of DFT points for water on Ni(111). This 9D PES allows the study of the influence of not only the internal degrees of freedom, but also the effects of impact sites and incident angles. QCT calculations confirmed the mode specificity in the dissociative chemisorption of D_2O observed in a recent experiment[16] and validated our reduced-dimensional model.[16, 19, 20] These results also uncovered the influence of the reaction path topography at different impact sites and substantial roles played by translational energy both parallel and perpendicular to the surface. The dependence of the reactant modes and incident angles can be rationalized by the SVP model, underscoring the importance of the reaction coordinate at the transition state. The present PIP-NN approach is systematic and applicable to high-dimensional PES construction for surface reactions, which is expected to stimulate future experimental and theoretical studies towards a quantitative understanding of multidimensional surface reaction dynamics.

Acknowledgements: We thank Dr. Morten Hundt and Prof. Rainer Beck for discussions about experimental conditions. This work was funded by the National

Science Foundation (CHE-0910828 and CHE-1462109 to HG). Parts of the calculations were performed at the National Energy Research Scientific Computing (NERSC) Center.

References:

[1] G. A. Somorjai, *Introduction to Surface Chemistry and Catalysis*. (Wiley, New York, 1994).
[2] G.-J. Kroes, Science **321**, 794 (2008).
[3] G.-J. Kroes, Phys. Chem. Chem. Phys. **14**, 14966 (2012).
[4] A. Gross, Surf. Sci. Rep. **32**, 291 (1998).
[5] G.-J. Kroes, A. Gross, E.-J. Baerends, M. Scheffler and D. A. McCormack, Acc. Chem. Res. **35**, 193 (2002).
[6] L. B. F. Juurlink, D. R. Killelea and A. L. Utz, Prog. Surf. Sci. **84**, 69 (2009).
[7] S. Nave, A. K. Tiwari and B. Jackson, J. Phys. Chem. A **118**, 9615 (2014).
[8] L. B. F. Juurlink, P. R. MaCabe, R. R. Smith, C. L. DeCologero and A. L. Utz, Phys. Rev. Lett. **83**, 868 (1999).
[9] R. R. Smith, D. R. Killelea, D. F. DelSesto and A. L. Utz, Science **304**, 992 (2004).
[10] L. B. F. Juurlink, R. R. Smith, D. R. Killelea and A. L. Utz, Phys. Rev. Lett. **94**, 208303 (2005).
[11] P. Maroni, D. C. Papageorgopoulos, M. Sacchi, T. T. Dang, R. D. Beck and T. R. Rizzo, Phys. Rev. Lett. **94**, 246104 (2005).
[12] D. R. Killelea, V. L. Campbell, N. S. Shuman and A. L. Utz, Science **319**, 790 (2008).
[13] R. Bisson, M. Sacchi and R. D. Beck, Phys. Rev. B **82**, 121404(R) (2010).
[14] B. L. Yoder, R. Bisson and R. D. Beck, Science **329**, 553 (2010).
[15] L. Chen, H. Ueta, R. Bisson and R. D. Beck, Faraday Disc. **157**, 285 (2012).
[16] P. M. Hundt, B. Jiang, M. van Reijzen, H. Guo and R. D. Beck, Science **344**, 504 (2014).
[17] G. P. Krishnamohan, R. A. Olsen, G.-J. Kroes, F. Gatti and S. Woittequand, J. Chem. Phys. **133**, 144308 (2010).
[18] S. Manzhos and K. Yamashita, Surf. Sci. **604**, 555 (2010).
[19] B. Jiang, X. Ren, D. Xie and H. Guo, Proc. Natl. Acad. Sci. USA **109**, 10224 (2012).
[20] B. Jiang, J. Li, D. Xie and H. Guo, J. Chem. Phys. **138**, 044704 (2013).
[21] X. J. Shen, A. Lozano, W. Dong, H. F. Busnengo and X. H. Yan, Phys. Rev. Lett. **112**, 046101 (2014).
[22] F. Nattino, H. Ueta, H. Chadwick, M. E. van Reijzen, R. D. Beck, B. Jackson, M. C. van Hemert and G.-J. Kroes, J. Phys. Chem. Lett. **5**, 1294 (2014).
[23] B. Jackson, F. Nattino and G.-J. Kroes, J. Chem. Phys. **141**, 054102 (2014).
[24] P. A. Thiel and T. E. Madey, Surf. Sci. Rep. **7**, 211 (1987).
[25] M. A. Henderson, Surf. Sci. Rep. **46**, 1 (2002).
[26] B. Jiang, D. Xie and H. Guo, Chem. Sci. **4**, 503 (2013).
[27] G. Kresse and J. Furthmuller, Phys. Rev. B **54**, 11169 (1996).
[28] G. Kresse and J. Furthmuller, Comp. Mater. Sci. **6**, 15 (1996).
[29] P. E. Blochl, Phys. Rev. B **50**, 17953 (1994).
[30] H. J. Monkhorst and J. D. Pack, Phys. Rev. B **13**, 5188 (1976).
[31] J. P. Perdew, K. Burke and M. Ernzerhof, Phys. Rev. Lett. **77**, 3865 (1996).

[32] J. P. Perdew, J. A. Chevary, S. H. Vosko, K. A. Jackson, M. R. Pederson, D. J. Singh and C. Fiolhais, Phys. Rev. B **46**, 6671 (1992).
[33] B. Jiang and H. Guo, J. Phys. Chem. C **118**, 26851 (2014).
[34] B. Jiang and H. Guo, J. Chem. Phys. **141**, 034109 (2014).
[35] Z. Xie and J. M. Bowman, J. Chem. Theo. Comp. **6**, 26 (2010).
[36] B. Jiang and H. Guo, J. Chem. Phys. **139**, 054112 (2013).
[37] J. Li, B. Jiang and H. Guo, J. Chem. Phys. **139**, 204103 (2013).
[38] B. Jiang and H. Guo, Phys. Chem. Chem. Phys. **16**, 24704 (2014).
[39] C. Diaz, R. A. Olsen, H. F. Busnengo and G. J. Kroes, J. Phys. Chem. C **114**, 11192 (2010).
[40] B. Jiang, R. Liu, J. Li, D. Xie, M. Yang and H. Guo, Chem. Sci. **4**, 3249 (2013).
[41] W. L. Hase, R. J. Duchovic, X. Hu, A. Komornicki, K. F. Lim, D.-H. Lu, G. H. Peslherbe, K. N. Swamy, S. R. V. Linde, A. Varandas, H. Wang and R. J. Wolf, Quantum Chemistry Program Exchange Bulletin **16**, 671 (1996).
[42] X. Hu, W. L. Hase and T. Pirraglia, J. Comp. Chem. **12**, 1014 (1991).
[43] W. L. Hase, in *Encyclopedia of Computational Chemistry*, edited by N. L. Alinger (Wiley, New York, 1998), Vol. 1, pp. 399.
[44] T. Liu, B. Fu and D. H. Zhang, Sci. China: Chem. **57**, 147 (2014).
[45] B. Jackson and S. Nave, J. Chem. Phys. **135**, 114701 (2011).
[46] T. Liu, B. Fu and D. H. Zhang, J. Chem. Phys. **141**, 194302 (2014).
[47] B. Jiang and H. Guo, J. Chem. Phys. **138**, 234104 (2013).
[48] B. Jiang and H. Guo, J. Phys. Chem. C **117**, 16127 (2013).
[49] H. Guo and B. Jiang, Acc. Chem. Res. **47**, 3679 (2014).
[50] D. R. Killelea and A. L. Utz, Phys. Chem. Chem. Phys. **15**, 20545 (2013).
[51] P. M. Holmblad, J. Wambach and I. Chorkendorff, J. Chem. Phys. **102**, 8255 (1995).
[52] See Supplemental Material [url], which includes Refs. [53-71]
[53] D. R. Lide, *CRC Handbook of Chemistry and Physics*, Internet Version 2005 ed. (CRC Press, Boca Raton, FL, 2005).
[54] G. Henkelman, B. P. Uberuaga and H. Jonsson, J. Chem. Phys. **113**, 9901 (2000).
[55] T. B. Blank, S. D. Brown, A. W. Calhoun and D. J. Doren, J. Chem. Phys. **103**, 4129 (1995).
[56] L. M. Raff, R. Komanduri, M. Hagan and S. T. S. Bukkapatnam, *Neural Networks in Chemical Reaction Dynamics*. (Oxford University Press, Oxford, 2012).
[57] S. Lorenz, M. Scheffler and A. Gross, Phys. Rev. B **73**, 115431 (2006).
[58] S. Manzhos and T. Carrington Jr., J. Chem. Phys. **125**, 194105 (2006).
[59] J. Behler, S. Lorenz and K. Reuter, J. Chem. Phys. **127**, 014705 (2007).
[60] J. Behler, Phys. Chem. Chem. Phys. **13**, 17930 (2011).
[61] J. Chen, X. Xu and D. H. Zhang, J. Chem. Phys. **138**, 154301 (2013).
[62] J. Chen, X. Xu, X. Xu and D. H. Zhang, J. Chem. Phys. **138**, 221104 (2013).
[63] J. Li and H. Guo, Phys. Chem. Chem. Phys. **16**, 6753 (2014).
[64] A. Li and H. Guo, J. Chem. Phys. **140**, 224313 (2014).
[65] M. H. Beale, M. T. Hagan and H. B. Demuth, *Neural Network Toolbox™ 7 User's Guide*. (The MathWorks, Inc., Natick, MA, 2010).
[66] I. Goikoetxea, J. Beltran, J. Meyer, J. I. Juaristi, M. Alducin and K. Reuter, New J. Phys. **14**, 013050 (2012).
[67] J. Meyer, Ph. D. Thesis, Freie Universitat Berlin, 2011.

[68] G.-M. Greuel, G. Pfister and H. Schönemann, (SINGULAR 3-1-6 ---A computer algebra system for polynomial computations, 2012, see http://www.singular.uni-kl.de).
[69] M. T. Hagan and M. B. Menhaj, IEEE Trans. Neural Networks **5**, 989 (1994).
[70] G. Füchsel, J. C. Tremblay and P. Saalfrank, J. Chem. Phys. **141**, 094704 (2014).
[71] Z.-H. Zhou, J. Wu and W. Tang, Art. Intel. **137**, 239 (2002).

Figure captions:

Figure 1. (a) Fixed-site barrier height (in eV) map in the smallest symmetry irreducible triangle within the approximate C_{6v} symmetry. (b-d) Fixed-site contour plots of the PES as a function of the vertical distance of H_2O COM (z_0) and the distance between the dissociating H atom and COM of the molecule (r), with other coordinates fully relaxed. The saddle point geometries are inserted in the right upper corner.

Figure 2. The initial lateral coordinates distribution for reactive trajectories in the irreducible triangle at different normal incident energies.

Figure 3. QCT dissociation probabilities of $D_2O(v_1, v_2, v_3)$ in normal incidence on the 9D and 6D PESs as a function of translational energy (upper panel) and total energy (lower panel). v_1, v_2, and v_3 denote the symmetric stretching, bending, and asymmetric stretching modes of D_2O, respectively. The total energy is relative to the asymptotic potential plus the zero-point energy of D_2O.

Figure 4. Dissociation probabilities of D_2O with nozzle temperatures at 573K (E_t=13.94 kcal/mol), 673K (E_t=15.68 kcal/mol), and 773K (E_t=17.71 kcal/mol), as a function of the incident angle, with the total translational energy fixed (upper panel) and the normal component of translational energy fixed (lower panel).

Fig. 1

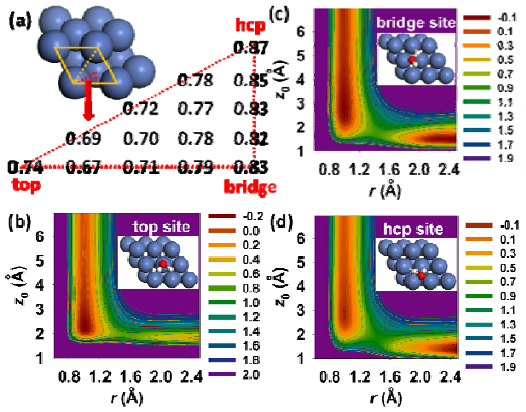
(a)
hcp
0.87
0.78 0.85
0.72 0.77 0.83
0.69 0.70 0.78 0.82
0.74 0.67 0.71 0.79 0.83
top
bridge
(c)
bridge site
(b)
top site
(d)
hcp site
z_0 (Å)
r (Å)
0.8 1.2 1.6 2.0 2.4

Fig. 2

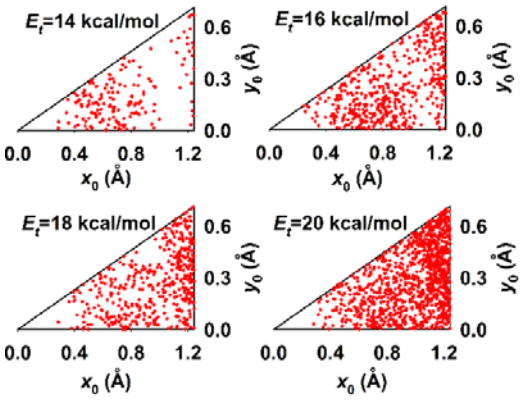
E_t=14 kcal/mol
E_t=16 kcal/mol
E_t=18 kcal/mol
E_t=20 kcal/mol
0.0
0.3
0.6
y_0 (Å)
0.0
0.4
0.8
1.2
x_0 (Å)

Figure 3

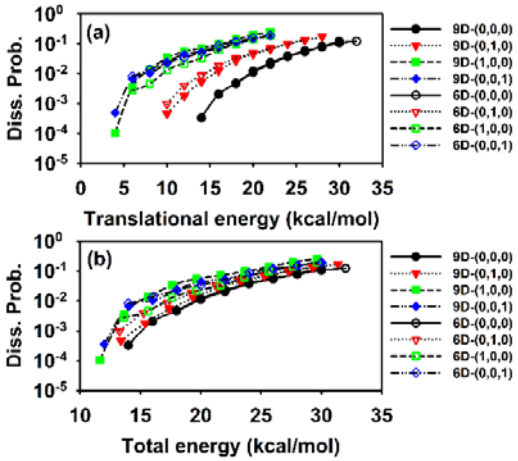
(a)
Diss. Prob.
Translational energy (kcal/mol)
(b)
Diss. Prob.
Total energy (kcal/mol)
9D-(0,0,0)
9D-(0,1,0)
9D-(1,0,0)
9D-(0,0,1)
6D-(0,0,0)
6D-(0,1,0)
6D-(1,0,0)
6D-(0,0,1)

Fig. 4

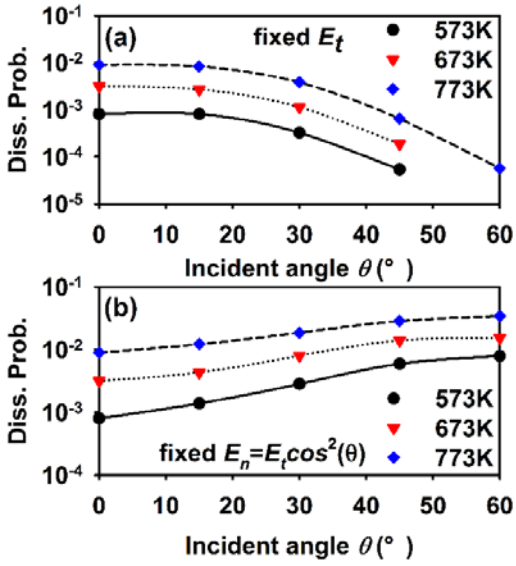
(a)
fixed E_t
573K
673K
773K
Diss. Prob.
10^{-1}
10^{-2}
10^{-3}
10^{-4}
10^{-5}
0
10
20
30
40
50
60
Incident angle θ(°)
(b)
fixed $E_n=E_t\cos^2(\theta)$
573K
673K
773K
Diss. Prob.
10^{-1}
10^{-2}
10^{-3}
10^{-4}
0
10
20
30
40
50
60
Incident angle θ(°)